# Electrophysiological correlates of the brain's intrinsic large-scale functional architecture

Biyu J. He*†, Abraham Z. Snyder*‡, John M. Zempel‡, Matthew D. Smyth§, and Marcus E. Raichle*†‡¶‖

Departments of *Radiology, ‡Neurology, §Neurosurgery, ¶Anatomy and Neurobiology, and ‖Biomedical Engineering, Washington University School of Medicine, St. Louis, MO 63110

Contributed by Marcus E. Raichle, August 4, 2008 (sent for review June 25, 2008)

**Spontaneous fluctuations in the blood-oxygen-level-dependent (BOLD) signals demonstrate consistent temporal correlations within large-scale brain networks associated with different functions. The neurophysiological correlates of this phenomenon remain elusive. Here, we show in humans that the slow cortical potentials recorded by electrocorticography demonstrate a correlation structure similar to that of spontaneous BOLD fluctuations across wakefulness, slow-wave sleep, and rapid-eye-movement sleep. Gamma frequency power also showed a similar correlation structure but only during wakefulness and rapid-eye-movement sleep. Our results provide an important bridge between the large-scale brain networks readily revealed by spontaneous BOLD signals and their underlying neurophysiology.**

electrocorticography | fMRI | functional connectivity | human | sleep

Spontaneous slow (<0.1 Hz) fluctuations in the blood-oxygen-level-dependent (BOLD) signals of functional magnetic resonance imaging (fMRI) appear to reflect a fundamental aspect of the brain's organization (1, 2). These fluctuations are temporally covariant within large-scale functional brain networks, such as those associated with sensorimotor (1), language (3), attention (4), and executive (5) functions as well as the "default network" (6). These covariant relations (i.e., correlation structures) of spontaneous BOLD signals exist during restful waking (1, 3–6), task performance (3, 7), sleep (8), and even general anesthesia (2). Furthermore, their integrity appears to be essential to normal brain function (7). However, in contrast to evoked BOLD responses (9–12), the electrophysiological basis of these spontaneous covariant BOLD fluctuations is unknown. Here, we investigated this question in five patients with intractable epilepsy undergoing evaluation with surgically implanted grids of subdural electrodes. Each patient underwent about a week of continuous video-monitored electrocorticography (ECoG) for the purpose of determining the epileptic focus before surgical resection.

The present analyses were based on ECoG data recorded in three distinct arousal states: (*i*) extended awake periods during which patients were in bed or seated, typically watching TV, eating, or engaged in social interactions; (*ii*) slow-wave sleep (SWS); and (*iii*) rapid-eye-movement (REM) sleep. Representative ECoG data are shown in supporting information (SI) Fig. S1. Resting-state (maintaining visual fixation) BOLD fMRI was acquired in a separate session either before or after surgical intervention. Patient information and data details are included in Table S1. In what follows, we present analyses using four different strategies to compare the correlation structures of BOLD and ECoG signals.

## Results

**Correlation Structures of Spontaneous BOLD Signal and Slow Cortical Potential.** In the first three analyses, we focused on the sensorimotor network, because the ECoG electrodes provided adequate coverage of the sensorimotor network in all presently studied patients but much poorer coverage of the other networks known to exhibit covariant BOLD fluctuations. For each patient, we first computed a voxel-wise BOLD correlation map of the sensorimotor network (Fig. 1 and Fig. S2; for methods, see *SI Text*). Electrodes then were categorized according to the underlying BOLD correlation map. Electrodes within the sensorimotor network as defined by this map ($Z$-score $> 3$, $P < 0.05$) were labeled "sensorimotor." Electrodes outside this network ($Z$-score $\leq 0$; see *Methods*) were labeled

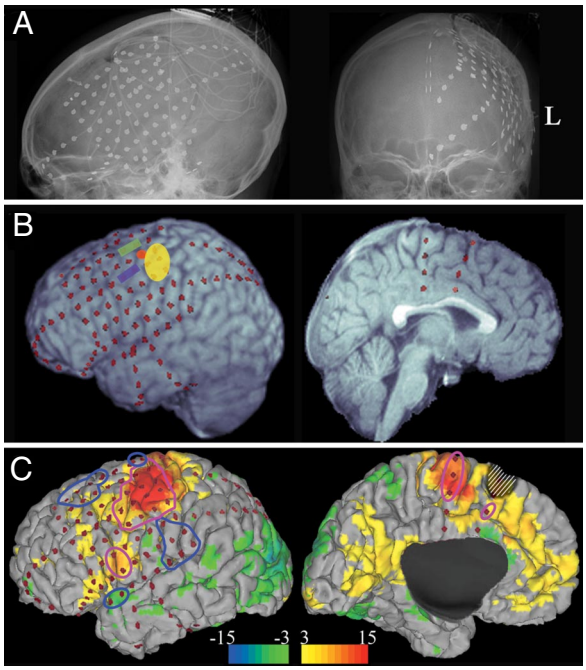


**Fig. 1.** Spatial topography of electrode coverage and sensorimotor network in Patient 1. (*A*) Radiograph showing electrode placements. (*B*) Three-dimensional rendering of anatomical MRI and projection of electrode locations onto the three-dimensional surface. Clinical mapping of the sensorimotor cortex is indicated by color patches. Red indicates hand motor area based on median nerve somatosensory evoked potential (SSEP); yellow indicates hand sensory area based on SSEP; blue indicates facial twitching in response to cortical stimulation; and green indicates hand grasp in response to cortical stimulation. (*C*) BOLD sensorimotor correlation map ($Z$-score, thresholded at $P < 0.05$, corrected for multiple comparisons) and electrode locations overlaid on the pial surface reconstructed from anatomical MRI. Two bad electrodes in the anterior temporal strip were eliminated. Four sensorimotor ROIs (delineated by magenta contours) and four control ROIs (blue contours) were determined in this patient. The cross-hatching indicates the epileptogenic zone that was subsequently resected.

Author contributions: B.J.H., A.Z.S., J.M.Z., and M.E.R. designed research; B.J.H., J.M.Z., and M.D.S. performed research; B.J.H., A.Z.S., and J.M.Z. analyzed data; and B.J.H., A.Z.S., J.M.Z., M.D.S., and M.E.R. wrote the paper.

The authors declare no conflict of interest.

Freely available online through the PNAS open access option.

See Commentary on page 15641.

†To whom correspondence may be addressed at: Washington University School of Medicine, 4525 Scott Avenue, St. Louis, MO 63110. E-mail: bhea@wustl.edu or marc@npg.wustl.edu.

This article contains supporting information online at www.pnas.org/cgi/content/full/0807010105/DCSupplemental.

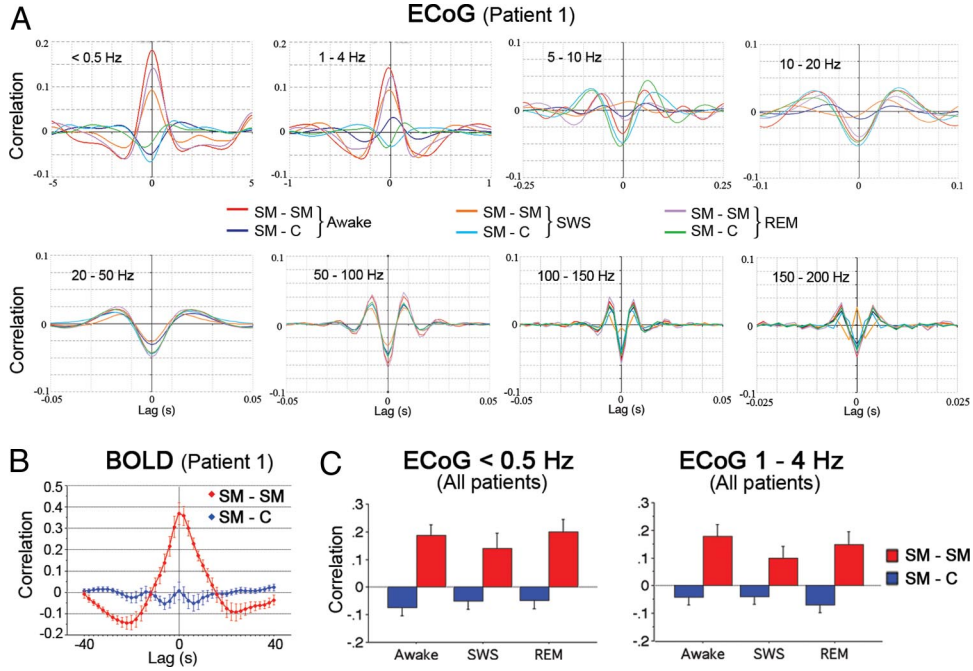


**Fig. 2.** ROI-pair cross-correlations computed using ECoG and BOLD signals. (*A*) Patient 1: lagged cross-correlation functions were computed by using ECoG signal filtered in eight frequency bands for all possible sensorimotor (SM)-SM ($n = 6$) and SM-control (C) ($n = 16$) ROI pairs. ROI pairs of similar type were averaged together after Fisher's *r*-to-*z* transformation. Red hues indicate SM-SM, and blue/green hues indicate SM-C. (*B*) Patient 1: BOLD lagged cross-correlation functions were averaged separately for SM-SM (red) and SM-C (blue) ROI pairs. (*C*) Combining data over all patients: peak ECoG cross-correlation values (within ± 500-ms lag) as a function of ROI-pair type (SM-SM vs. SM-C) and arousal state (awake, SWS, and REM). Two-way ANOVA yielded a highly significant main effect of ROI-pair type (<0.5 Hz: $F_{1,47} = 20.1$, $P < 0.0001$; 1–4 Hz: $F_{1,47} = 17.8$, $P = 0.0001$). Neither the effect of arousal state nor the interaction of ROI-pair type × arousal state was significant ($P > 0.1$). All error bars denote SEM.

"control." To increase signal-to-noise ratio, in the first two analyses, we defined sensorimotor and control regions of interest (ROIs) as contiguous groups of sensorimotor and control electrodes and averaged ECoG and BOLD signals within each ROI. Several ROIs of each type were defined in all patients (Fig. 1 and Fig. S2).

In the first analysis, we computed lagged cross-correlation functions for all possible sensorimotor-sensorimotor and sensorimotor-control ROI pairs using BOLD and filtered ECoG signals. Because the sensorimotor ROIs were located within a common network defined by BOLD correlation structure, whereas the control ROIs were outside this network, BOLD correlations between sensorimotor ROIs should be, by definition, higher than correlations between a sensorimotor ROI and a control ROI (see Fig. 2*B* and Fig. S3). The question was whether some type of electrophysiological activity may similarly differentiate sensorimotor-sensorimotor from sensorimotor-control correlations. To pursue this question, ECoG signals filtered in eight different frequency bands (<0.5 Hz, 1–4 Hz, 5–10 Hz, 10–20 Hz, 20–50 Hz, 50–100 Hz, 100–150 Hz, and 150–200 Hz) were used to compute the lagged correlation functions (see *Methods*). These correlation functions then were compared across the two types of ROI pairs.

ECoG activity in the two slowest frequency bands (<0.5-Hz and 1–4-Hz bands) distinguished sensorimotor-sensorimotor from sensorimotor-control ROI pairs: the sensorimotor-sensorimotor ROI pairs were positively correlated, whereas the sensorimotor-control ROI pairs were negatively or not correlated. Remarkably, this distinction was present in all arousal states (Fig. 2*A* and Fig. S3). Similar findings were absent in higher frequency bands (Fig. 2*A* and Fig. S4). These results were consistent across all five subjects. Considering only the waking data, across all patients, 86% of the sensorimotor-sensorimotor correlation functions (using either <0.5-Hz or 1–4-Hz band ECoG) had a positive peak with an *r* value >0.1 in the lag range within ± 0.5 s; in contrast, only 19% (<0.5-Hz band) or 16% (1–4-Hz band) of sensorimotor-control correlations showed similar positive peaks. For statistical results, see Fig. 2*C*. Importantly, this difference in slow ECoG signal correlation between sensorimotor-sensorimotor and sensorimotor-control ROI pairs cannot be accounted for by a difference in their respective inter-ROI distances, because the distribution of inter-ROI distances was the same for the two groups of ROI pairs (Fig. 3).

Whereas these analyses filtered the ECoG signal in eight different frequency bands, and thus had a crude spectral resolution, converging results from an independent analysis employing coherence measurement with a fine spectral resolution are presented in Fig. S5 (for methods, see *SI Examining the relation between BOLD and ECoG correlation structures as a function of ECoG frequency*).

In the second analysis, to assess the similarity between the correlation structures of BOLD signal and slow ECoG activity quantitatively, we plotted ECoG (filtered at <0.5 Hz, Fig. 4*A*; filtered at 1–4 Hz, Fig. 4*b*) vs. BOLD correlation values across all sensorimotor-sensorimotor and sensorimotor-control ROI pairs in all patients. Highly significant correlations between BOLD and ECoG correlation measures were found for ECoG signals in the <0.5-Hz and 1–4-Hz bands from all three arousal states (all $P <$ 0.002), thereby demonstrating a correspondence between the correlation structures of spontaneous BOLD signal and slow (<4 Hz) cortical potential (SCP) recorded by ECoG.

In the third analysis, we computed spatial correlations between BOLD and slow ECoG (<0.5-Hz band) correlation maps to compare their spatial patterns on an electrode-by-electrode basis. Voxel-wise BOLD correlation maps were spatially sampled by the electrode coverage to compare with ECoG correlation maps (for each electrode, the corresponding BOLD correlation value was evaluated by averaging over a 5-mm-radius sphere centered on that electrode, excluding voxels outside the pial surface). For correlation map examples, see Fig. 5*A*. All sensorimotor and control electrodes were used as seed electrodes; thus, this analysis did not depend on ROIs. We found that the great majority of BOLD and ECoG

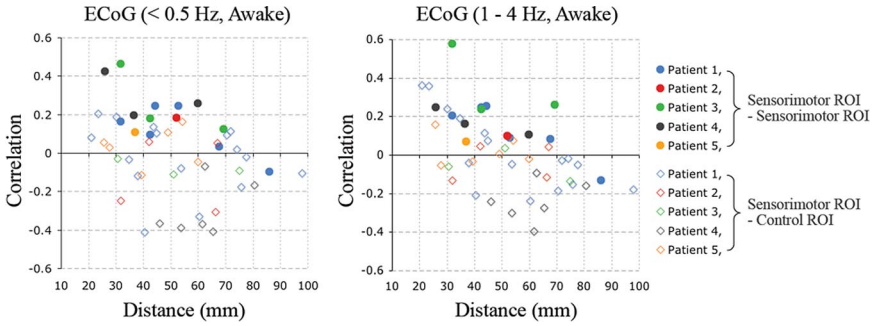


**Fig. 3.** Effect of inter-ROI distance on ECoG peak cross-correlation values (within lag of ± 500 ms). (*Left*) <0.5-Hz band. (*Right*) 1–4-Hz band. ECoG data were from the waking state. Each ROI pair is represented by one symbol. ● indicates sensorimotor-sensorimotor ROI pair. ◇ indicates sensorimotor-control ROI pair.

correlation maps obtained by seeding at the same electrode were highly similar (98.3% of such comparisons had a spatial correlation value that was significant at the $P < 0.05$ level, uncorrected for potential dependence of signals at neighboring electrodes). Next, we examined the similarity of correlation maps obtained with different seed electrodes within the sensorimotor system, with the outcome measure being the mean spatial correlation averaged over pairs of seed electrodes. As shown in Fig. 5*B* and Fig. S6, this measure was significantly positive, regardless of whether the spatial correlations were computed within modality (BOLD:BOLD or ECoG:ECoG) or across modalities (BOLD:ECoG). In contrast, the spatial correlation measures comparing maps obtained by seeding at "sensorimotor" electrodes vs. those obtained by seeding at "control" electrodes were, on average, around zero, again regardless of whether the comparison was within or across modalities. These spatial correlation results cannot be accounted for by the effect of distance between seed electrodes (see Fig. S7). They confirmed the previous finding that the correlation structures of spontaneous BOLD and slow (<0.5 Hz) ECoG signals are similar, at least within the framework of the sensorimotor system.

In the fourth analysis, to extend our findings beyond the sensorimotor system, we evaluated the similarity of BOLD and slow ECoG (<0.5-Hz band) covariance structures using an eigenvector decomposition strategy (for details of the method, see *SI Statistical testing of covariance matrix similarity by eigenvector decomposition*). In brief, this strategy tested whether the eigenvectors accounting for more variance in the BOLD data also accounted for more variance in the ECoG data, which, if true, would strongly reinforce the impression of a similarity between the BOLD and ECoG covariance structures derived from our other analyses. This analysis

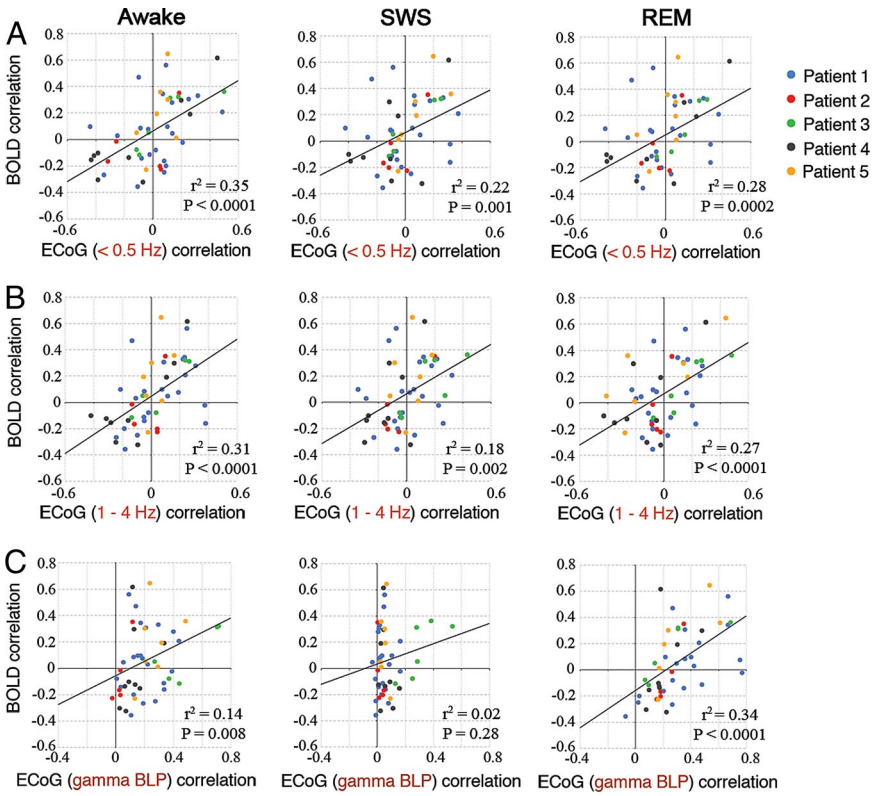


**Fig. 4.** BOLD vs. ECoG cross-correlation function peak values. Peak correlations of filtered (<0.5 Hz and 1–4 Hz) ECoG activity were evaluated for lags in the range ± 500 ms. Peak correlations of BOLD and γ-BLP (both sampled at 2-s interval) were evaluated at zero-lag. Each ROI pair is represented by one symbol. All sensorimotor-sensorimotor and sensorimotor-control ROI pairs from all patients are shown. In Patient 2, the ECoG derivation was modified Laplacian; in all other patients, it was average reference. (*A*) <0.5-Hz ECoG. (*B*) 1–4-Hz EcoG. (*C*) γ-BLP EcoG. *P* values represent the significance of the measured correlation between BOLD and ECoG peak correlations.

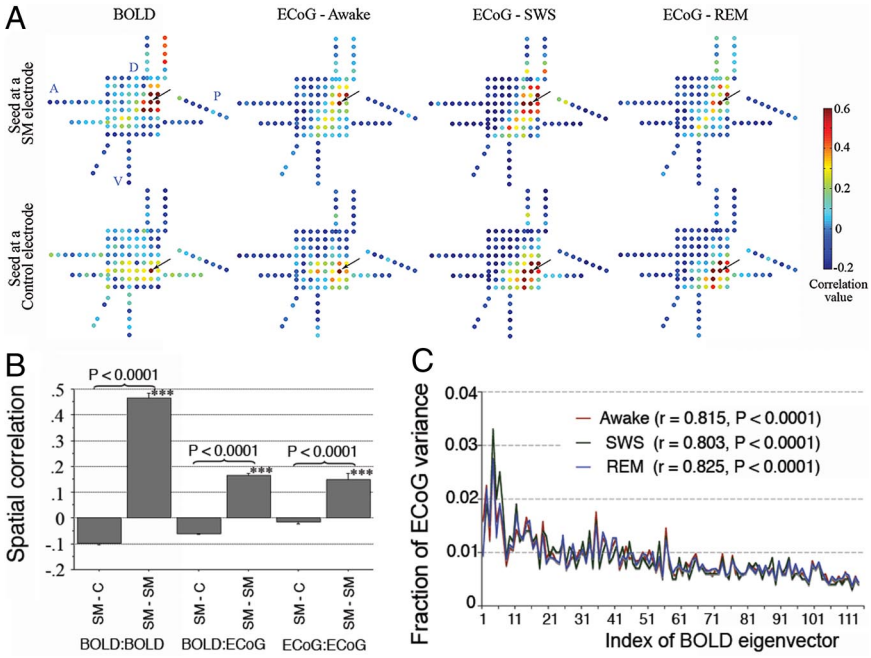


**Fig. 5.** Similarity of BOLD and ECoG (<0.5-Hz band) correlation structures assessed by spatial correlation and eigenvector decomposition strategies in Patient 1. (*A*) Raw representative BOLD and ECoG (<0.5 Hz) correlation maps that were used for spatial correlation analyses. Each dot represents one electrode. The arrow points to the seed electrode. Color represents Fisher's *z*-transformed correlation value between each electrode and the seed electrode, computed by using BOLD signal or <0.5-Hz ECoG signal from each arousal state. BOLD correlation maps were spatially sampled by the electrode coverage to compare with ECoG correlation maps. The maps in the top row seed at a same sensorimotor (SM) electrode, and those in the bottom row seed at a control (C) electrode. Note that these two seed electrodes are separated only by 2 cm. A, anterior; D, dorsal; P, posterior; V, ventral. This two-dimensional presentation of the electrode grid was extrapolated from Fig. 1. (*B*) Statistical results of spatial correlation analysis. Spatial correlations were computed between two BOLD correlation maps (BOLD:BOLD), between two ECoG correlation maps (ECoG:ECoG), or between a BOLD correlation map and an ECoG correlation map (BOLD:ECoG). Each bar represents the mean spatial correlation averaged over seed-electrode pairs. SM-C indicates that one correlation map was obtained by seeding at an SM electrode and the other map by seeding at a C electrode. SM-SM indicates that both maps were obtained by seeding at an SM electrode. Error bars denote SEM. ***: significant nonzero mean spatial correlation ($P < 0.0001$; one-sample *t* test). The over-bracketed *P* values indicate unpaired *t* tests comparing seed electrodes within (SM-SM) vs. across (SM-C) functional systems. ECoG data were from the waking state. Comparable results were obtained in all patients and for ECoG data from all states of arousal (Fig. S6). (*C*) Eigenvector decomposition analysis comparing BOLD and ECoG (from all three states) covariance structures. The ordinate shows the fraction of ECoG variance captured by eigenvectors derived by diagonalization of the BOLD covariance matrix. These eigenvectors were sorted by the rank-ordering of their corresponding eigenvalues (index shown in the abscissa), such that the eigenvector with the smallest index was associated with the largest eigenvalue, and hence accounted for the most variance in the BOLD data. The variable range of the abscissa reflects the number of eigenvectors, which is the same as the number of usable electrodes in each patient. The decreasing trend of the plot indicates that eigenvectors accounting for more BOLD variance also accounted for more ECoG variance. The statistical significance of the covariance structure similarity (tested by Spearman rank order correlation) is listed in the key. Comparable results were obtained in all patients (Fig. S8).

included all ECoG electrodes providing technically satisfactory recording, and hence was independent of the distinction between sensorimotor and nonsensorimotor networks. Statistical significance was assessed using a nonparametric test (Spearman rank order correlation) requiring no correction or qualification. The results again showed that the covariance structures corresponding to the two types of signals (BOLD and <0.5-Hz ECoG) were similar in all five patients for ECoG data acquired in all three arousal states (all $P < 0.005$; Fig. 5*C* and Fig. S8).

**Correlation Structures of Spontaneous BOLD Signal and Gamma Band-Limited Power.** So far, we have demonstrated a correspondence between the correlation structures of spontaneous BOLD signal and SCP representing the slowest component of raw ECoG signals (<4 Hz). However, power of gamma frequency (>30 Hz) has not only been demonstrated to correlate with BOLD in stimulus-evoked activity (9–12) but has been shown to remain coherent in its spontaneous fluctuations at distances up to 1 cm, unlike spontaneous raw gamma oscillations that are correlated only locally (13). Hence, we tested in an additional analysis whether gamma (50–100 Hz) band-limited power (γ-BLP) also had a correlation structure similar to spontaneous BOLD signals. Fig. 4*C* shows scatter plots of BOLD correlations against γ-BLP correlations across all ROI pairs. A significant correlation with BOLD was found for γ-BLP in waking ($P = 0.008$) and REM ($P < 0.0001$) data but not in SWS ($P = 0.28$) data. We note that the lack of correspondence during SWS was not attributable to a reduction in the amount of gamma frequency power, which was invariant across arousal states (Fig. S9) (14). Consistent results from spatial correlation analysis comparing BOLD and γ-BLP correlation maps are shown in Fig. S10.

Given the correlation between γ-BLP and BOLD signal in stimulus-evoked responses (9–12), it is possible that the waking γ-BLP result presented herein was partly driven by environmental stimuli present during data recording. However, a similar result was obtained for γ-BLP during REM sleep, in which neuronal activity arises completely from within. Therefore, it appears that endogenous brain activity during REM sleep, and presumably also wakefulness, modulates γ-BLP in a spatial pattern similar to that of spontaneous BOLD fluctuations. Equally telling, γ-BLP during SWS did not show a similar correlation structure. This result is consistent with the view that coherent patterns in gamma frequency activity are related to conscious experiences (15, 16) that are more prevalent in wakefulness and REM sleep than in SWS (17, 18). An alternative but not contradictory explanation is that the bistability of thalamocortical circuits between up and down states during SWS

(19) is responsible both for the fading of consciousness and for the collapse of gamma power correlations.

Interestingly, whereas the BOLD and SCP correlations included both negative and positive values, γ-BLP correlations were mainly positive (Fig. 4). One possible explanation is that the removal of global signal in BOLD signal processing and the use of average reference in ECoG analysis forced the appearance of negative BOLD and SCP correlations, whereas no equivalent maneuver was done in the BLP analysis. However, negative SCP correlations also emerged when modified Laplacian montage was used (see results from Patient 2 in Fig. 4 and *SI Supplementary Note 1*); in this case, there was no numerical mandate of negative correlations. An alternative explanation is that positive correlations of BOLD/SCP signals indicate that the two regions are in the same network, which, as if crossing a threshold, "enables" the covariant γ-BLP relation. By contrast, no γ-BLP relation exists when this threshold is not crossed. Undoubtedly, a better understanding of this phenomenon awaits future investigation.

## Discussion

To summarize, we have identified two types of neurophysiological signals that demonstrate a similar correlation structure to that of the spontaneous fMRI BOLD signal: SCP and γ-BLP. For SCP, the correspondence with BOLD was state-invariant. For γ-BLP, the correspondence was present in wakefulness and REM sleep but not in SWS. This leads us to suggest that spontaneous fMRI BOLD signals and SCPs both reflect a fundamental stratum of the brain's intrinsic organization that transcends levels of consciousness. The more labile state-dependent structures of γ-BLP, though similar, appear to be built on scaffolding provided by the more fundamental processes represented in the BOLD signals and the SCPs.

A remaining question regards whether the spontaneous BOLD signal, SCP, and γ-BLP are correlated on a time-varying basis. This could not be directly addressed in the present study because of the lack of simultaneous BOLD and ECoG recordings. However, because these three signals have comparable frequency ranges (see *SI Supplementary Note 2*), it is not unreasonable to speculate that they may indeed be temporally coherent. Unfortunately, to date, relevant empirical observations remain scarce. Nevertheless, it has been shown in anesthetized rats that spontaneously fluctuating total hemoglobin concentration and low-pass filtered local field potential are temporally correlated**; when the anesthesia level was deepened to produce burst-suppression ECoG patterns, the spontaneous fluctuating blood flow faithfully followed bursts of ECoG activity at a frequency of ~0.1 Hz (20). Whereas nonneuronal factors have been shown to contribute to spontaneous BOLD signal variance (21–23), these studies and the present work suggest an important neural origin of these signals. Furthermore, numerous early EEG studies have shown that the negative shift of SCP occurs in response to various task demands much in the same way as the BOLD signal activation does [for a recent review, see the article by Khader *et al.* (24)]. Hence, SCP may be a fundamental neural basis of the BOLD signal—a basis for the spontaneous BOLD fluctuations and task-evoked BOLD responses alike.

Our results and the foregoing interpretations are consistent with well-established neuroanatomical and neurophysiological observations. The negative shift of SCPs reflects depolarization of apical dendrites in cortical superficial layers (e.g., by excitatory nonspecific thalamic inputs) (25, 26). Therefore, spontaneous SCP and the correlated BOLD signal fluctuations likely reflect endogenous fluctuations of cortical excitability within functional systems. (For a discussion on the relation between SCP and the "up-and-down states," which also reflects fluctuations of cortical excitability, see *SI Supplementary Note 3*.) Interestingly, glial cells become depolarized by local excitatory dendritic activity and contribute to negative SCP regardless of cortical depth because of their syncytial connections (26, 27); these glial cells also concurrently take up synaptically released glutamate and contribute to locally increased glycolysis, which, in turn, increases the BOLD signal (28).

It has been shown that the trough of SCP is associated with increased power of higher frequency field potentials (29) as well as increased multiple-unit activity (26). Hence, the correlated noise in unit recordings (30) may be regulated by the correlated spontaneous fluctuations of SCPs confined within the large-scale brain functional networks. Furthermore, a long-established line of research showing the influence of spontaneous variations of SCPs on psychological performance is especially intriguing. Tasks presented on the negative shifts of spontaneous SCP fluctuations are solved faster (31) and more accurately (32) and had a lower sensory threshold (33), supporting the role of spontaneous activity in facilitating responses to stimuli. Similar investigations in the fMRI domain have only begun to blossom (34, 35).

## Methods

**Subjects.** Five patients undergoing surgical treatment for intractable epilepsy participated in the study. To localize epileptogenic zones, patients underwent a craniotomy for subdural placement of electrode grids and strips, followed by 1 to 2 weeks of continuous video and ECoG monitoring. The placement of the electrodes and the duration of monitoring were determined entirely by clinical considerations. All patients gave informed consent according to the procedures established by Washington University Institutional Review Board. Exclusion criteria were (*i*) widespread interictal spike-and-wave discharges, (*ii*) age <10 years old, (*iii*) severely impaired cognitive capability, (*iv*) diffuse brain tissue abnormality (e.g., tuberous sclerosis, cerebral palsy), and (*v*) limited electrode coverage (e.g., only temporal lobe strips) (see Table S1 for demographic and clinical information).

**Electrophysiology Data Acquisition.** The electrode arrays (typically 8 × 8, 4 × 5, or 2 × 5) and strips (typically 1 × 6 or 1 × 8) consisted of platinum electrodes 4 mm in diameter (2.3 mm exposed) with a center-to-center distance of 10 mm between adjacent electrodes (AD-TECH Medical Instrument Corporation). ECoG signals were recorded using a standard clinical monitoring system (Proamp; LaMont Medical Inc.; 0.1–500-Hz bandpass, 18-dB/octave roll-off). Sampling frequency was 512 Hz for Patients 1 through 4 and 200 Hz for Patient 5. Noisy electrodes and electrodes overlying pathological tissue (including both the primary epileptogenic zone and areas showing active interictal spike-wave discharges) were eliminated from all analyses.

Artifact-free and interictal-spike-free segments of ECoG data were clipped off the clinical recordings obtained in three distinct arousal states: quiet wakefulness, SWS (stages 3/4), and REM sleep. The length of data segments ranged from 2.7 to 112 min (mean = 20.6 min). Arousal state determination was based on the conjunction of ECoG and video recordings. REM sleep was identified by (*i*) active eye movements in the video record and/or the electro-oculogram and (*ii*) low power in the <4-Hz band. Time courses of <4-Hz BLP were computed over entire nighttime records using fast Fourier transform applied to half-overlapping windows of 1 s in length. Periods with <4-Hz BLP as low as the waking state were selected, excluding those preceded by a sharp (as opposed to gradual) transition from SWS (marked by high <4-Hz BLP) which were more likely to represent arousal/awakening rather than REM sleep. Total lengths of data collected for each patient are listed in Table S1.

Methods for MRI data acquisition and generation of voxel-wise BOLD correlation maps are described in SI.

**Electrode Localization.** Plain radiographs and computed tomography (CT) scans were acquired postoperatively with the subdural electrodes in place to define the electrode positions in relation to the skull. The CT images were coregistered to subject's own anatomical MR image and then to the atlas-representative image. The Talairach coordinates of the center of each electrode then were determined using a locally developed automated procedure. Three-dimensional renderings of the pial surface were generated from atlas-transformed anatomical MR images using MRIcro (http://www.sph.sc.edu/comd/rorden/mricro.html) (Fig. 1*B*) and Freesurfer (http://surfer.nmr.mgh.harvard.edu) (Fig. 1*C*). Displays showing BOLD correlation maps and electrode locations overlaid on the pial surface (from Freesurfer) were generated using CARET (http://brainmap.wustl.edu/caret).

For each electrode, the corresponding BOLD sensorimotor correlation map *Z*-score (thresholded at a significance level of $P < 0.05$ corrected for multiple comparisons; see SI) was evaluated by averaging over a 5-mm-radius sphere

**Jones MO, *et al.* (2007) 37th Annual Meeting of the Society for Neuroscience, November 3–7, 2007, San Diego, abstr 89.16.

centered on the electrode, excluding voxels outside the pial surface. Electrodes with a *Z*-score greater than 3 were classified as ''sensorimotor.'' Electrodes with a *Z*-score equal to or less than 0 were classified as ''control.'' A group of contiguous ''sensorimotor'' electrodes constituted a sensorimotor ROI. A group of contiguous ''control'' electrodes constituted a control ROI. The distance between two ROIs was computed in Talairach space as the distance between the center of mass of each group of electrodes. The distances between ROIs were carefully controlled such that (*i*) all ROIs were separated by >2 cm so as to focus on large-scale brain functional connectivity and (*ii*) the distribution of inter-ROI distances was comparable between the sensorimotor-sensorimotor and sensorimotor-control groups (see *SI Supplementary Note 4* and Fig. 3). In addition, widespread strong negative correlations to the sensorimotor network were avoided as control ROIs because their physiological meaning is as yet unclear.

**ECoG Correlation Analyses and Comparison with BOLD Correlation Structure.** ECoG signals were re-referenced to the common mean before further analyses. In Patient 2, results obtained using such average reference derivation were compared with those obtained using a modified Laplacian derivation (see *SI Supplementary Note 1*). A 60-Hz notch filter was used for ECoG signals filtered in 50 to 100 Hz.

**Analysis of Filtered Regional ECoG Signals.** Analysis was performed separately in eight different frequency ranges: <0.5 Hz, 1–4 Hz, 5–10 Hz, 10–20 Hz, 20–50 Hz, 50–100 Hz, 100–150 Hz, and 150–200 Hz. Regional ECoG time series were extracted by averaging over the electrodes constituting each ROI and were made zero-mean and detrended. Data were Fourier transformed, and the cross- and auto-spectra corresponding to ROI pairs were computed and averaged over half-overlapping windows of 10-s length across the entire data set (data segments from the same arousal state were averaged together). The averaged cross- and auto-spectra for each ROI pair were filtered in each of the aforementioned frequency ranges (18 dB/octave) and inverse Fourier transformed to yield the lagged cross- and auto-covariance functions for each frequency band. The lagged cross-covariance functions then were normalized to obtain the lagged cross-correlation functions. This approach is similar to that used by von Stein *et al.* (36). Lagged cross-correlation functions are shown in Fig. 2*A* and Figs. S3 and S4.

**Analysis of Regional $\gamma$-BLP Signals.** Regional $\gamma$-BLP time series (2-s sampling interval) were obtained by fast Fourier transform of successive half-overlapping 4-s windows and summing over frequency bins in the range of 50 to 100 Hz (excluding 60-Hz bin). For each ROI pair and arousal state, lagged cross-correlation functions were conventionally computed in the time domain for each data segment and averaged across segments from the same arousal state.

**Analyses of Regional BOLD Signals.** Regional BOLD time series were computed by averaging over voxels under electrodes constituting each ROI (see *Electrode Localization*). For each ROI pair, lagged BOLD cross-correlation functions were conventionally computed in the time domain for each fMRI run and then averaged across runs.

Statistical testing of all cross-correlations was performed after application of Fisher's *r*-to-*z* transform.

**Spatial Correlation of Temporal Correlation Maps.** Spatial correlation was used to assess spatial similarity of correlation maps (4). Here, correlation maps were obtained by computing temporal correlations of the signal (BOLD or ECoG) at one (seed) electrode against all other electrodes. Thus, we obtained $r^B_{ik}$ and $r^E_{ik}$, the (zero-lag) temporal correlation map corresponding to seed electrode *i*, where *k* indexes all other electrodes and the superscript indicates modality (BOLD or ECoG). ECoG correlation maps ($r^E_{ik}$) were computed on signals that were low-pass filtered at <0.5 Hz and down-sampled to 8 Hz (Fig. 5 *A* and *B* and Fig. S6) or by using $\gamma$-BLP time series (Fig. S10). The $r^B_{ik}$ and $r^E_{ik}$ were subjected to Fisher's *r*-to-*z* transformation to obtain $z^B_{ik}$ and $z^E_{ik}$. Within-modality and cross-modality spatial correlations, $R^{B:B}_{ij}$, $R^{E:E}_{ij}$, and $R^{B:E}_{ij}$, then were computed for pairs of seed electrodes. Thus, for seed electrodes *i* and *j*, the spatial correlation was computed as

$$R^{X:Y}_{ij} = \frac{\sum_{k\neq i,j} (z^X_{ik} - \bar{z}^X_i)(z^Y_{jk} - \bar{z}^Y_j)}{\sqrt{\sum_{k\neq i} (z^X_{ik} - \bar{z}^X_i)^2 \sum_{k\neq j} (z^Y_{jk} - \bar{z}^Y_j)^2}},$$

where *X* and *Y* each range over *B* (BOLD) and *E* (ECoG).

**Statistical Testing of Covariance Matrix Similarity by Eigenvector Decomposition.** This approach tests similarity of BOLD vs. ECoG covariance structures. It is complementary to the foregoing spatial correlation analysis. Detailed methods are included in SI.

**ACKNOWLEDGMENTS.** This research was supported by a National Institutes of Health Grant NS06833.

1. Biswal B, Yetkin FZ, Haughton VM, Hyde JS (1995) Functional connectivity in the motor cortex of resting human brain using echo-planar MRI. *Magn Reson Med* 34:537–541.
2. Vincent JL, et al. (2007) Intrinsic functional architecture in the anaesthetized monkey brain. *Nature* 447:83–86.
3. Hampson M, Peterson BS, Skudlarski P, Gatenby JC, Gore JC (2002) Detection of functional connectivity using temporal correlations in MR images. *Hum Brain Mapp* 15:247–262.
4. Fox MD, Corbetta M, Snyder AZ, Vincent JL, Raichle ME (2006) Spontaneous neuronal activity distinguishes human dorsal and ventral attention systems. *Proc Natl Acad Sci USA* 103:10046–10051.
5. Seeley WW, *et al.* (2007) Dissociable intrinsic connectivity networks for salience processing and executive control. *J Neurosci* 27:2349–2356.
6. Greicius MD, Krasnow B, Reiss AL, Menon V (2003) Functional connectivity in the resting brain: A network analysis of the default mode hypothesis. *Proc Natl Acad Sci USA* 100:253–258.
7. He BJ, *et al.* (2007) Breakdown of functional connectivity in frontoparietal networks underlies behavioral deficits in spatial neglect. *Neuron* 53:905–918.
8. Horovitz SG, *et al.* (2008) Low frequency BOLD fluctuations during resting wakefulness and light sleep: A simultaneous EEG-fMRI study. *Hum Brain Mapp* 29:671–682.
9. Logothetis NK, Pauls J, Augath M, Trinath T, Oeltermann A (2001) Neurophysiological investigation of the basis of the fMRI signal. *Nature* 412:150–157.
10. Mukamel R, *et al.* (2005) Coupling between neuronal firing, field potentials, and FMRI in human auditory cortex. *Science* 309:951–954.
11. Niessing J, *et al.* (2005) Hemodynamic signals correlate tightly with synchronized gamma oscillations. *Science* 309:948–951.
12. Shmuel A, Augath M, Oeltermann A, Logothetis NK (2006) Negative functional MRI response correlates with decreases in neuronal activity in monkey visual area V1. *Nat Neurosci* 9:569–577.
13. Leopold DA, Murayama Y, Logothetis NK (2003) Very slow activity fluctuations in monkey visual cortex: Implications for functional brain imaging. *Cereb Cortex* 13:422–433.
14. Steriade M, Contreras D, Amzica F, Timofeev I (1996) Synchronization of fast (30–40 Hz) spontaneous oscillations in intrathalamic and thalamocortical networks. *J Neurosci* 16:2788–2808.
15. Singer W (2001) Consciousness and the binding problem. *Ann NY Acad Sci* 929:123–146.
16. Rodriguez E, et al. (1999) Perception's shadow: Long-distance synchronization of human brain activity. *Nature* 397:430–433.
17. Llinas R, Ribary U (1993) Coherent 40-Hz oscillation characterizes dream state in humans. *Proc Natl Acad Sci USA* 90:2078–2081.
18. Hobson JA, Pace-Schott EF, Stickgold R (2000) Dreaming and the brain: Toward a cognitive neuroscience of conscious states. *Behav Brain Sci* 23:793–842, discussion 904–1121.
19. Massimini M, Huber R, Ferrarelli F, Hill S, Tononi G (2004) The sleep slow oscillation as a traveling wave. *J Neurosci* 24:6862–6870.
20. Golanov EV, Yamamoto S, Reis DJ (1994) Spontaneous waves of cerebral blood flow associated with a pattern of electrocortical activity. *Am J Physiol* 266:R204–R214.
21. Birn RM, Diamond JB, Smith MA, Bandettini PA (2006) Separating respiratory-variation-related fluctuations from neuronal-activity-related fluctuations in fMRI. *Neuroimage* 31:1536–1548.
22. Shmueli K, *et al.* (2007) Low-frequency fluctuations in the cardiac rate as a source of variance in the resting-state fMRI BOLD signal. *Neuroimage* 38:306–320.
23. Wise RG, Ide K, Poulin MJ, Tracey I (2004) Resting fluctuations in arterial carbon dioxide induce significant low frequency variations in BOLD signal. *Neuroimage* 21:1652–1664.
24. Khader P, Schicke T, Roder B, Rosler F (2008) On the relationship between slow cortical potentials and BOLD signal changes in humans. *Int J Psychophysiol* 67:252–261.
25. Mitzdorf U (1985) Current source-density method and application in cat cerebral cortex: Investigation of evoked potentials and EEG phenomena. *Physiol Rev* 65:37–100.
26. Birbaumer N, Elbert T, Canavan AG, Rockstroh B (1990) Slow potentials of the cerebral cortex and behavior. *Physiol Rev* 70:1–41.
27. Goldring S (1974) in *Handbook of Electroencephalography and Clinical Neurophysiology*, ed. Remond A (Elsevier, Amsterdam), pp. 12–24.
28. Raichle ME, Mintun MA (2006) Brain work and brain imaging. *Annu Rev Neurosci* 29:449–476.
29. Vanhatalo S, *et al.* (2004) Infraslow oscillations modulate excitability and interictal epileptic activity in the human cortex during sleep. *Proc Natl Acad Sci USA* 101:5053–5057.
30. Averbeck BB, Latham PE, Pouget A (2006) Neural correlations, population coding and computation. *Nat Rev Neurosci* 7:358–366.
31. Stamm JS, Whipple SC, Born J (1987) Effects of spontaneous cortical slow potentials on semantic information processing. *Int J Psychophysiol* 5:11–18.
32. Stamm JS, Gillespie O (1978) in *Multidisciplinary Perspectives in Event-Related Brain Potential Research*, ed. Otto DA (US Environmental Protection Agency, Washington, DC), pp. 410–415.
33. Devrim M, Demiralp T, Kurt A, Yucesir I (1999) Slow cortical potential shifts modulate the sensory threshold in human visual system. *Neurosci Lett* 270:17–20.
34. Boly M, *et al.* (2007) Baseline brain activity fluctuations predict somatosensory perception in humans. *Proc Natl Acad Sci USA* 104:12187–12192.
35. Fox MD, Snyder AZ, Vincent JL, Raichle ME (2007) Intrinsic fluctuations within cortical systems account for intertrial variability in human behavior. *Neuron* 56:171–184.
36. von Stein A, Chiang C, Konig P (2000) Top-down processing mediated by interareal synchronization. *Proc Natl Acad Sci USA* 97:14748–14753.